Measurement of the Cross Section for Prompt Isolated Diphoton Production in $p\overline{p}$ Collisions at $\sqrt{s} = 1.96$ TeV

Costas Vellidis for the CDF Collaboration
Fermi National Accelerator Laboratory, Batavia, IL, USA

This article reports a measurement of the cross section of prompt isolated photon pair production in $p\overline{p}$ collisions at a total energy $\sqrt{s} = 1.96$ TeV using data of 5.36 fb^{-1} integrated luminosity collected with the CDF II detector at the Fermilab Tevatron. The measured cross section, differential in basic kinematic variables, is compared with three perturbative QCD predictions, a leading order (LO) parton shower calculation and two next-to-leading order (NLO) calculations. The NLO calculations reproduce most aspects of the data. By including photon radiation from quarks before and after hard scattering, the parton shower prediction becomes competitive with the NLO predictions.

1. Introduction

The measurement of the production cross section of two energetic isolated central photons (diphotons) in high energy hadron collisions is important for testing standard model (SM) predictions in the domain of searches for undiscovered particles and new physics. Photons originating from hard collisions of hadrons ("direct" or "prompt" photons) are an ideal probe for testing perturbative Quantum ChromoDynamics (pQCD) and soft-gluon resummation methods implemented in theoretical calculations because they do not interact with other final state particles, and their energies and directions can be measured with high precision in modern electromagnetic calorimeters. Prompt diphoton production with large invariant mass creates an irreducible background in searches for a low mass Higgs boson decaying into a photon pair [1], as well as in searches for new phenomena, such as new heavy resonances [2], extra spatial dimensions [3, 4] or cascade decays of heavy new particles [5]. Precise measurements of the diphoton production differential cross sections for various kinematic variables and their theoretical understanding are thus very important for these searches.

The basic mechanisms of prompt diphoton production in hadron collisions are quark-antiquark annihilation $q\overline{q} \rightarrow \gamma\gamma$, quark-gluon scattering $gq \rightarrow \gamma\gamma q$, and gluon-gluon fusion $gg \rightarrow \gamma\gamma$. The respective basic diagrams are shown in Fig. 1. At the Tevatron, the dominant mechanism is quark-antiquark annihilation. In quark-gluon scattering, most of the time at least one of the two photons is emitted almost parallel to the scattered quark. Contributions from this mechanism are therefore suppressed by requiring isolated prompt photons. Each mechanism can be modeled by calculating the respective matrix element for the specific event kinematics. Matrix element calculations of Leading Order (LO) in the strong coupling are relatively simple and are thus implemented in advanced parton shower Monte Carlo (MC) event generators [6–8], which allow for gluon and photon radiation as well as multiple interactions in the colliding beams. By including radiation before and after the hard scattering, parton shower generators take into account soft gluon and photon emissions, thus resulting in an effective resummation of all of the Leading Logarithmic (LL) terms in the cross section to all orders of the strong and electromagnetic couplings constants. Next-to-Leading Order (NLO) calculations [9–11] additionally include one-loop corrections at the cost of not featuring realistic multi-particle event representations as the LO generators do. Recent NLO calculations include an analytical resummation of the cross section for initial-state gluon radiation to all orders in the strong coupling constant [11], reaching a higher logarithmic accuracy than in the parton shower Monte Carlo generators. By this method, all soft gluon emissions in the initial state are taken into account, and reliable predictions for the low diphoton transverse momentum region are possible. A fixed-order NLO calculation implemented by the DIPHOX program [9] also accounts for the case where a final state quark loses almost all of its energy to the photon detected in the event [diagram (e) of Fig. 1] [12]. This process is called "fragmentation" and, in contrast to final state photon radiation in parton showering, it involves non-perturbative calculations. One or both photons in the event may come from fragmentation. The case where both photons come from fragmentation of a single quark is also possible, but is not included in calculations, as in this case the photons are nearly collinear and thus non-isolated most of the time.

Diphoton measurements have been previously conducted at fixed-target [13] and collider experiments [14–17]. The most recent measurements [16, 17] were compared with the same pQCD calculations examined in the present work and large discrepancies were found between the data and a LO matrix element calculation supplemented with a parton shower model, suitable for simulation of the backgrounds in searches of a low mass Higgs boson and of new phenomena. This work shows that the inclusion of photons radiated from initial and final state quarks drastically improves the comparison of the parton shower calculation with the data.
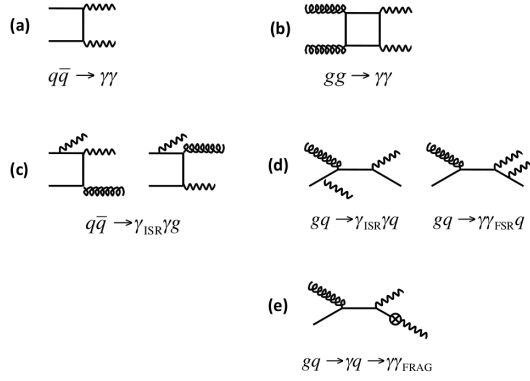
Figure 1: Basic diagrams for prompt diphoton production: (a-b) direct, (c-d) one-photon radiation from an initial- (ISR) or final-state quark (FSR), (e) fragmentation where one photon is emitted along the direction of a final-state quark taking almost all of its energy. The symbol $\otimes$ denotes the non-perturbative mechanism of the fragmentation process (FRAG).

2. Measurement

The reported measurement was conducted using data of total integrated luminosity 5.36 fb^{-1} collected with the Collider Detector at Fermilab (CDF) [18] at the Tevatron $p\overline{p}$ collider. CDF is composed of a central spectrometer inside a 1.4 T magnetic field, surrounded by electromagnetic and hadronic calorimeters and muon detection chambers. The inner spectrometer measures charged particle tracks with a transverse momentum (p_{T}) precision of $\Delta p_{\mathrm{T}}/p_{\mathrm{T}}^2 = 0.07\%(\mathrm{GeV/c})^{-1}$. The central calorimeters cover the region $|\eta| < 1.1$, with an electromagnetic (hadronic) energy resolution of $\sigma(E_{\mathrm{T}})/E_{\mathrm{T}} = 13.5\%/\sqrt{E_{\mathrm{T}}(\mathrm{GeV})} \oplus 1.5\%$ $(\sigma(E_{\mathrm{T}})/E_{\mathrm{T}} = 50\%/\sqrt{E_{\mathrm{T}}(\mathrm{GeV})} \oplus 3\%)$ and a tower segmentation of $\Delta\eta \times \Delta\phi \simeq 0.1 \times 15°$. Photons are reconstructed in clusters of up to three towers [19]. χ^2 criteria are imposed on the profile of the shower to match expected patterns. Two main cuts are applied: (i) the photon transverse energy is required to be $E_{\mathrm{T}} \geq 17$ GeV for the first photon in the event and $E_{\mathrm{T}} \geq 15$ GeV for the second photon; (ii) the calorimeter isolation energy in the isolation cone around each photon [20] is required to be less than 2 GeV.

The background from γ+jet and dijet events, where one or two jets are faking a photon, is subtracted with a method using the track isolation as the discriminant between signal and background [21]. It is based on the substantial difference of the track isolation distribution for signal photons (nearly exponential) and for background photons (nearly flat). The advantages of this method are that (i) it has little sensitivity to multiple interactions in the colliding beams, so that the signal-background separation does not degrade at high instantaneous luminosity, and (ii) it has high efficiency and good track momentum resolution, implying minimal degradation of the signal-background separation due to instrumental effects. The signal fraction is determined by summing the probabilities of an event to be pure signal, pure background, or mixed photon pair. These probabilities are obtained by solving a 4×4 matrix equation using the observation value (0 or 1) for all four combinations of the leading or sub-leading photon having track isolation below or above 1 GeV/c as an input. The matrix is constructed from the E_{T}-dependent efficiencies of signal and background photons passing the track isolation cut. A threshold cut of 1 GeV/c is determined by maximizing the separation between signal and background. The efficiencies are determined from Monte Carlo (MC) γ+jet and dijet samples, which are produced using the PYTHIA event generator [6]. PYTHIA events are fully simulated through the detector and trigger and are reconstructed with the CDF II simulation and reconstruction software [22]. With this matrix technique the full correlations between the two photons in the event are properly taken into account. Tests are made for underlying event contributions in complementary cones to the photon reconstruction cone [23] and also using isolated tracks in dijet events. The systematic uncertainty in the signal fraction with this method is of the order of 15-20%.

The diphoton production cross section differential in a kinematic variable is obtained from the histogram of the estimated signal in the selected variable. The average cross section in a bin of the variable is determined by dividing the bin content by the trigger efficiency, the diphoton selection efficiency and acceptance, the integrated luminosity and the bin size. The diphoton trigger efficiency is derived from data [1]. It is consistent with 100%

over all of the kinematic range with a flat uncertainty of 3%. The selection efficiency is determined from data and MC with an iterative method. In the first pass the efficiency is determined from a fully simulated and reconstructed PYTHIA diphoton MC sample by dividing the number of events passing all selection cuts by the number of events passing only the kinematic cuts on the photon E_{T}, η, angular separation and isolation at the event generation level. The efficiency denominator is corrected for the "underlying event" from collision remnants which make the efficiency obtained from PYTHIA too high by removing events from the denominator through the isolation cut. This correction is derived by running PYTHIA with and without underlying event and amounts to a constant factor of 0.88 per event. A flat 6% uncertainty in the selection efficiency (3% per photon) accounts for possible inaccuracies in the PYTHIA model for the underlying event. The signal events of the data are corrected for the preliminary efficiency. The data are then used to reweight the PYTHIA events and obtain a more accurate representation of the true diphoton distribution. The efficiency is determined using the reweighted PYTHIA sample and corrected for luminosity dependence, derived from a comparison of the vertex multiplicity distribution in data and PYTHIA MC $Z^0 \to e^+e^-$ events. The systematic uncertainty in the efficiency resulting from the luminosity dependent correction grows linearly from 1.8% for $E_{\mathrm{T}} \leq 40$ GeV to 3% at $E_{\mathrm{T}} = 80$ GeV and remains constant above this point. Finally, a 6% constant uncertainty comes from the Tevatron integrated luminosity [24].

The $Z^0 \to e^+e^-$ sample is used for calibration by applying a "diphoton-like" event selection, i.e. by imposing a diphoton selection with the same trigger but allowing for a track associated with each of the two electromagnetic objects in the event. The electromagnetic energy scale in data and MC is corrected by tuning the $Z^0 \to e^+e^-$ mass peak to the world average [25] and a systematic uncertainty from this correction is estimated to grow linearly from 0 at $E_T \leq 40$ GeV up to 1.5% at $E_{\mathrm{T}} = 80$ GeV and remain constant above this point. The difference in the photon identification efficiency between data and MC is estimated from the $Z^0 \to e^+e^-$ sample [1] and added as a systematic uncertainty to the measurement. All systematic uncertainties in the cross section measurement are added in quadrature.

3. Predictions

The results of this measurement are compared with three theoretical calculations: (i) the fixed NLO predictions of the DIPHOX program [9] including parton fragmentations into photons [12], (ii) the predictions of the RESBOS program [11] where the cross section is accurate to NLO, but also has an analytical initial state soft gluon resummation, and (iii) the predictions of the PYTHIA program [6] which features a realistic representation of the physics events by including parton showering, Initial (ISR) and Final State Radiation (FSR) and an underlying event model. Diphoton events were selected from an inclusive γ+X PYTHIA sample (X=γ or jet), thus including the $q\bar{q} \to \gamma\gamma$ and $gg \to \gamma\gamma$ processes (56%) as well as the $q\bar{q} \to g\gamma\gamma_{\mathrm{ISR}}$, $gq \to q\gamma\gamma_{\mathrm{ISR}}$ and $gq \to q\gamma\gamma_{\mathrm{FSR}}$ processes (44%). This type of calculation effectively resums the cross section for gluon and photon radiation both in the initial and the final state. Fig. 2 shows the individual contributions to the cross section as a function of the diphoton invariant mass, transverse momentum and azimuthal difference. Initial-state radiation (ISR) photons, in particular, produce substantially different distributions than ME and final-state radiation (FSR) photons, having a harder transverse momentum spectrum and stronger low–$\Delta\phi$ tail in the azimuthal difference spectrum. In leading order, this can be attributed to the fact that FSR occurs in quark-gluon scattering [diagram (d) of Fig. 1], whereas ISR occurs both in $q\bar{q}$ annihilation [diagram (c) of Fig. 1] and quark-gluon scattering, and the luminosity of quark-gluon states falls off more rapidly with the parton momenta than the luminosity of $q\bar{q}$ states [9, 11]. Double radiation processes in minimum bias dijet events, such as $qq \to qq\gamma_{\mathrm{ISR/FSR}}\gamma_{\mathrm{ISR/FSR}}$, $q\bar{q} \to q\bar{q}\gamma_{\mathrm{ISR/FSR}}\gamma_{\mathrm{ISR/FSR}}$, $gq \to gq\gamma_{\mathrm{ISR/FSR}}\gamma_{\mathrm{ISR/FSR}}$, $q\bar{q} \to gg\gamma_{\mathrm{ISR}}\gamma_{\mathrm{ISR}}$ and $gg \to q\bar{q}\gamma_{\mathrm{FSR}}\gamma_{\mathrm{FSR}}$, were also examined but their overall contribution was estimated to only $\sim 3\%$ of the total, having no significant effect to any kinematical distribution. Therefore, these processes were not included in the PYTHIA calculation.

All calculations are subject to the experimental kinematic and isolation cuts. DIPHOX accounts for the $gg \to \gamma\gamma$ process in LO only. The predictions of RESBOS are restricted to the invariant mass range from $2m_b = 9$ GeV/c^2 to $2m_t = 350$ GeV/c^2, where m_b and m_t are the masses of the bottom and top quarks, respectively. NLO theoretical uncertainties are estimated by varying the fragmentation (in DIPHOX only), renormalization and factorization scales up and down by a factor of two relative to the default scale $\mu = M/2$ of DIPHOX and $\mu = M$ of RESBOS, and for the NLO PDF uncertainties (in both DIPHOX and RESBOS) by using the 20 CTEQ6.1M eigenvectors [26]. Theoretical uncertainties are shown only in the plots of the relative deviations of the data from each calculation, in the form (data−theory)/theory, as functions of the selected variable. No relative deviations are shown for the PYTHIA $\gamma\gamma$ calculation. The benchmark parton showering MC calculation, compared in detail with the data, is PYTHIA $\gamma\gamma + \gamma$j.
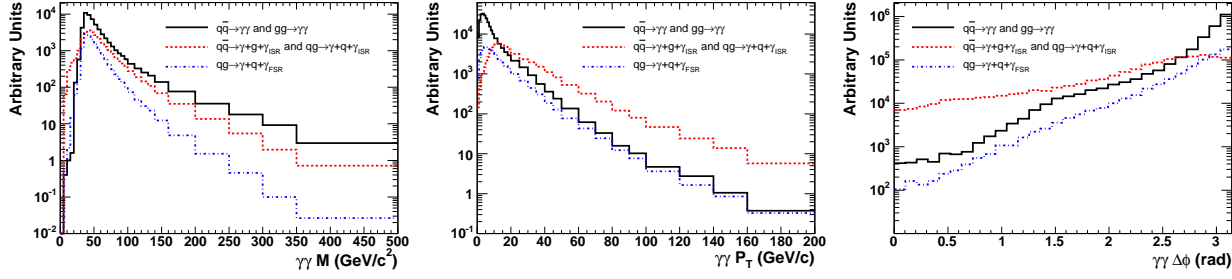
Figure 2: The individual contributions to the cross section from events where both photons are generated according to the PYTHIA diphoton matrix element and from events where one photon originates from initial or final state radiation, as functions of the diphoton mass (left), transverse momentum (middle) and azimuthal difference (right).

Table I: The total diphoton production cross section obtained from the measurement and from the theoretical calculations. The PYTHIA $\gamma\gamma$ calculation involves only the $q\bar{q} \to \gamma\gamma$ and $gg \to \gamma\gamma$ processes. The PYTHIA $\gamma\gamma + \gamma$j calculation includes also the $q\bar{q} \to \gamma\gamma g$ and $gq \to \gamma\gamma q$ processes.

	Cross section (pb)
Data	$12.47 \pm 0.21_{\text{stat}} \pm 3.74_{\text{syst}}$
RESBOS	$11.31 \pm 2.45_{\text{syst}}$
DIPHOX	$10.58 \pm 0.55_{\text{syst}}$
PYTHIA $\gamma\gamma + \gamma$j	9.19
PYTHIA $\gamma\gamma$	5.03

4. Results

The measured total cross section is shown in Table I together with the predictions from the three theoretical calculations. All three calculations are consistent with the size of the measured cross section within the experimental uncertainties.

Fig. 3 shows the comparison between the measured and predicted diphoton cross sections as functions of the diphoton invariant mass M, the diphoton transverse momentum P_{T} and the difference $\Delta\phi$ between the azimuthal angles of the two photons in the event. While the PYTHIA direct calculation ($\gamma\gamma$) fails to describe both the scale and shape of the data, including radiation brings the prediction in fair agreement with the data. In particular, radiation makes the P_{T} and $\Delta\phi$ distributions harder because of the presence of at least one hard jet in the final state of events in which one photon originates from radiation. The mass distributions show a reasonable agreement with the data for all predictions above the peak at 30 GeV/c^2, particularly in the region 80 GeV/c$^2 < M < 150$ GeV/c^2 relevant to searches for the Higgs boson [1]. However, all predictions underestimate the data around and below the peak. In the P_{T} spectrum all predictions underestimate the data in the region between 20 and 50 GeV/c, a feature also observed in the earlier measurements [9, 16]. For $P_{\text{T}}<20$ GeV/c, where soft gluon resummation is most important, only the RESBOS prediction describes the data. Discrepancies between data and theory are most prominent in the comparison of the measured and predicted distributions of $\Delta\phi$. In this case all three predictions fail to describe the data across the whole spectrum. Approaching $\Delta\phi = \pi$, where soft gluon processes are expected to manifest, the RESBOS prediction agrees better with the data. In the range 1.4 rad$<\Delta\phi<2.2$ rad only the PYTHIA prediction describes the data and remains closest to the data down to 1 rad. In the low $\Delta\phi$ tail, which corresponds to the region of low M (<50 GeV/c^2), all three predictions are lower than the data, although the DIPHOX prediction, by explictly including non-perturbative fragmentation, lies closer to the data for $\Delta\phi<1$ rad.

Fig. 4 shows the comparison between the measured and predicted diphoton cross sections as functions of the diphoton rapidity $Y_{\gamma\gamma}$, the cosine of the polar angle in the Collins-Soper frame $\cos\theta$ [27], and the ratio z of the subleading photon E_{T} to leading photon E_{T}. All three predictions agree fairly well with the measured $d\sigma/dY_{\gamma\gamma}$, $d\sigma/d\cos\theta$ and $d\sigma/dz$, within uncertainties. Exceptions are the predictions of all three calculations underestimating the data in the two ends of the $\cos\theta$ spectrum, where again gluon scattering processes and associated fragmentation are expected to dominate [11].

In general, all three calculations reproduce most of the main features of the data, as observed in the earlier

diphoton cross section measurements [16, 17]. However, depending on their approximations, they display differences with each other and with the data in certain kinematic regions. There is a problem common to all three calculations in the description of events with very low diphoton mass, low azimuthal distance and diphoton transverse momentum in the region of the so-called "Guillet shoulder" (20 GeV/c<P_T<50 GeV/c) [9]. Such events include fragmentation at a relatively high rate. The PYTHIA $\gamma\gamma$ calculation fails completely to describe the data both in the scale, where it is low by a factor of 2.5 (see Table I), and in the shape, particularly of the P_T, $\Delta\phi$ and z distributions, where it predicts a much softer spectrum than the data. This is in agreement with the conclusion of Ref. [16] which tested only PYTHIA $\gamma\gamma$ as a parton showering MC prediction.

5. Summary

In summary, the diphoton production cross section, differential in kinematic variables sensitive to the reaction mechanism, is measured using data corresponding to an integrated luminosity of 5.36 fb^{-1} collected with the CDF II detector. The high statistics of the measured sample allows for a higher precision scan over a much more extended phase space than previous measurements. The overall systematic uncertainty is limited to about 30%. The results of the measurement are compared with three state-of-the-art calculations, applying complementary techniques in describing the reaction. All three calculations, within their known limitations, reproduce the main features of the data, but none of them describes all aspects of the data. The inclusion of photon radiation in the initial and final states significantly improves the PYTHIA parton shower calculation (see the left-hand panels in Figures 3 and 4), which is suitable for background simulations in searches for a low mass Higgs boson and new phenomena.

Acknowledgments

References

1 T. Aaltonen *et al.* (CDF Collaboration), Phys. Rev. Lett. **103**, 061803 (2009); V. M. Abazov *et al.* (D0 Collaboration), Phys. Rev. Lett. **102**, 231801 (2009); G. Aad *et al.* (ATLAS Collaboration), arXiv:0901.0512 [hep-ex] (2009); G. L. Bayatian *et al.* (CMS Collaboration), J. Phys. G **34**, 995 (2007).

2 S. Mrenna and J. Willis, Phys. Rev. D **63**, 015006 (2001), and references therein.

3 M. C. Kumar, P. Mathews, V. Ravindran and A. Tripathi, Phys. Lett. B **672**, 45 (2009).

4 T. Aaltonen *et al.* (CDF Collaboration), Phys. Rev. Lett. **99**, 171801 (2007); T. Aaltonen *et al.* (CDF Collaboration), Phys. Rev. D **83**, 011102 (2011); The CMS Collaboration, J. High Energy Phys. 05 (2011) 085; The ATLAS Collaboration, arXiv:1107.0561v2 [hep-ex] (2011).

5 G. F. Giudice and R. Rattazzi, Phys. Rep. **322**, 419 (1999).

6 T. Sjöstrand, Comput. Phys. Commun. **82**, 74 (1994); S. Mrenna, Comput. Phys. Commun. **101**, 232 (1997).

7 G. Corcella, I. G. Knowles, G. Marchesini, S. Moretti, K. Odagiri, P. Richardson, M. H. Seymour and B. R. Webber, J. High Energy Phys. 01 (2001) 010.

8 S. Höche, S. Schumann and F. Siegert, Phys. Rev. **D81**, 034026 (2010).

9 T. Binoth, J. P. Guillet, E. Pilon and M. Werlen, Eur. Phys. J. **C16**, 311 (2000); T. Binoth, J. P. Guillet, E. Pilon and M. Werlen, Phys. Rev. **D63**, 114016 (2001).

10 Z. Bern, L. Dixon and C. Schmidt, Phys. Rev. **D66**, 074018 (2002).

11 C. Balazs, E. L. Berger, P. Nadolsky and C.-P. Yuan, Phys. Lett. **D637**, 235 (2006); C. Balazs, E. L. Berger, P. Nadolsky and C.-P. Yuan, Phys. Rev. **D76**, 013009 (2007); C. Balazs, E. L. Berger, P. Nadolsky and C.-P. Yuan, Phys. Rev. **D76**, 013008 (2007).

12 L. Bourhis, M. Fontannaz and J. P. Guillet, Eur. Phys. J. **C2**, 529 (1998).

13 E. Bonvin *et al.* (WA70 Collaboration), Z. Phys. C **41**, 591 (1989); Phys. Lett. B **236**, 523 (1990).

14 C. Albajar *et al.* (UA1 Collaboration), Phys. Lett. B **209**, 385 (1988).

15 J. Alitti *et al.* (UA2 Collaboration), Phys. Lett. B **288**, 385 (1992).

16 D. Acosta *et al.* (CDF Collaboration), Phys. Rev. Lett. **95**, 022003 (2005).

17 V. M. Abazov *et al.* (D0 Collaboration), Phys. Lett. B **690**, 108 (2010).

18 CDF II Collaboration, FERMILAB-PUB-96/90-E (1996); see also A. Sill *et al..*, Nucl. Instrum. Meth. A **447**, 1 (2000) and T. Affolder *et al..*, Nucl. Instrum. Meth. A **42586**, 249 (2004) for the spectrometer; L. Balka *et al..*, Nucl. Instrum. Meth. A **267**, 272 (1988) and S. Bertolucci *et al..*, Nucl. Instrum. Meth. A **267**, 301 (1988) for the central calorimeters.

19 T. Aaltonen *et al.*, arXiv.09105170v1 (to be published in Phys. Rev. D).

20 The calorimeter isolation is defined as the difference of the transverse energy $E_T = E\sin\theta$ in the isolation cone minus the transverse energy in the tower cluster of the photon. The isolation cone is defined to have a radius $R = \sqrt{(\Delta\eta)^2 + (\Delta\phi)^2} = 0.4$ around the axis of the shower profile, where $\eta = -\ln[\tan(\theta/2)]$ is the pseudo-rapidity, θ is the polar angle and ϕ the azimuth in the coordinate system of the laboratory with polar axis along the colliding beams and origin at the center of the detector. The isolation cut implies that the angular separation of the two photons is $\Delta R \geq 0.4$.

21 The track isolation is defined as the scalar sum of the transverse momenta $p_T = |\vec{p}|\sin\theta$ of all tracks originating from the primary vertex of the event and lying within the photon reconstruction cone.

22 E. Gerchtein and M. Paulini, CHEP-2003-TUMT005, arXiv:physics/0306031; the version of GEANT used for the detector simulation is 3.21, see the CERN Program Library Long Writeup W5013.

23 The complementary cone is defined by rotating the photon reconstruction cone by an azimuthal angle of 90° about the beam axis, keeping the polar angle fixed.

24 S. Klimenko, J. Konigsberg, and T.M. Liss, FERMILAB-FN-0741 (2003).

25 W.-M. Yao *et al.*, (Particle Data Group), J. Phys. G **33**, 2006.

26 J. Pumplin, D. R. Stump, J. Huston, H. L. Lai, P. Nadolsky and W. K. Tung, J. High Energy Phys. **0207**, 012 (2002).

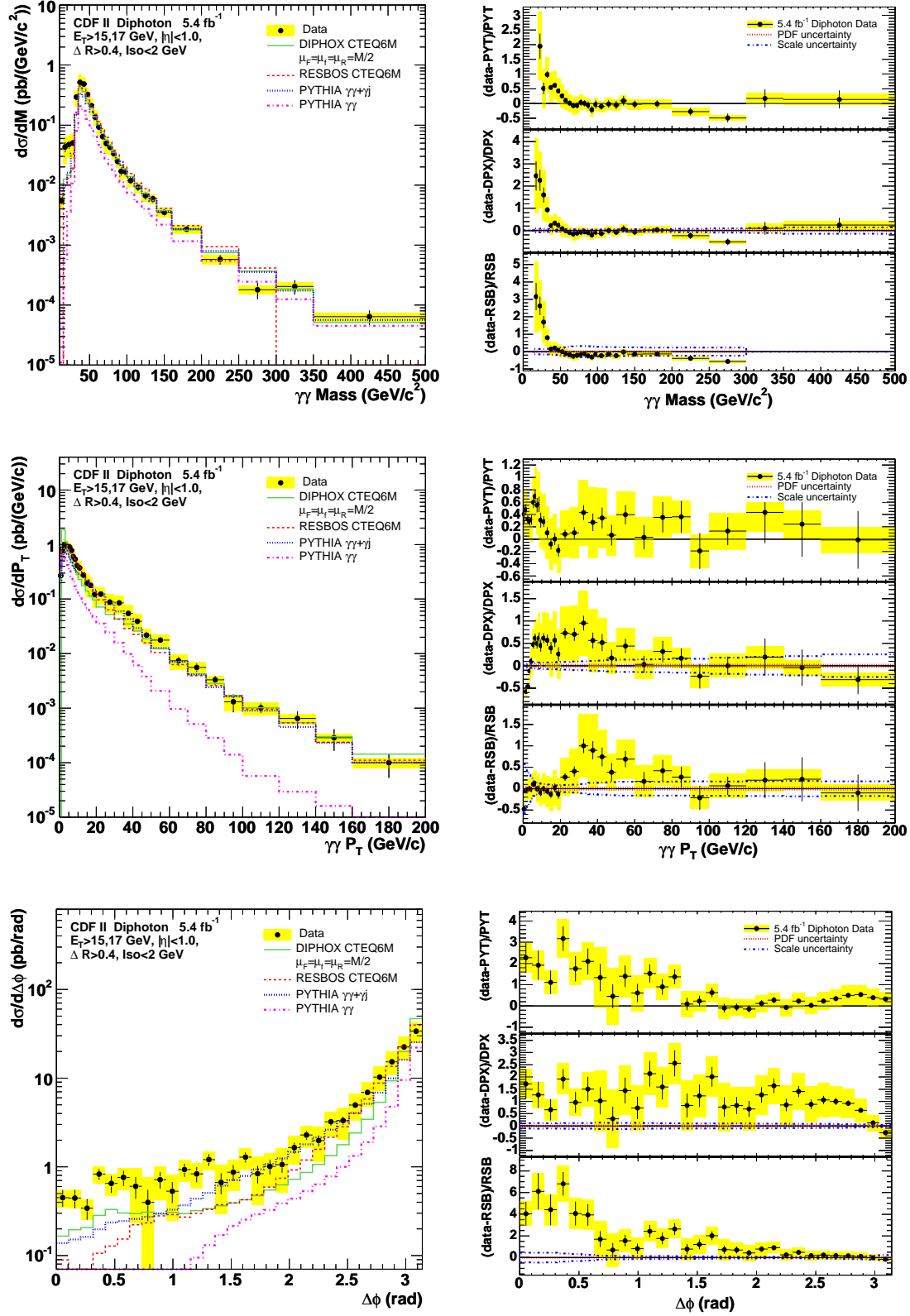27 J. C. Collins and D. E. Soper, Phys. Rev D **16**, 2219 (1977).

Figure 3: The measured differential cross sections compared with three theoretical predictions discussed in the text. The left windows show the absolute comparisons and the right windows show the fractional deviations of the data from the theoretical predictions. Fractional deviations for PYTHIA refer to the $\gamma\gamma+\gamma$j calculation. Note that the vertical axis scales differ between fractional deviation plots. The comparisons are made as functions of the diphoton mass (top), transverse momentum (middle) and azimuthal angle difference (bottom). The shaded area around the data points indicates the total systematic uncertainty of the measurement.
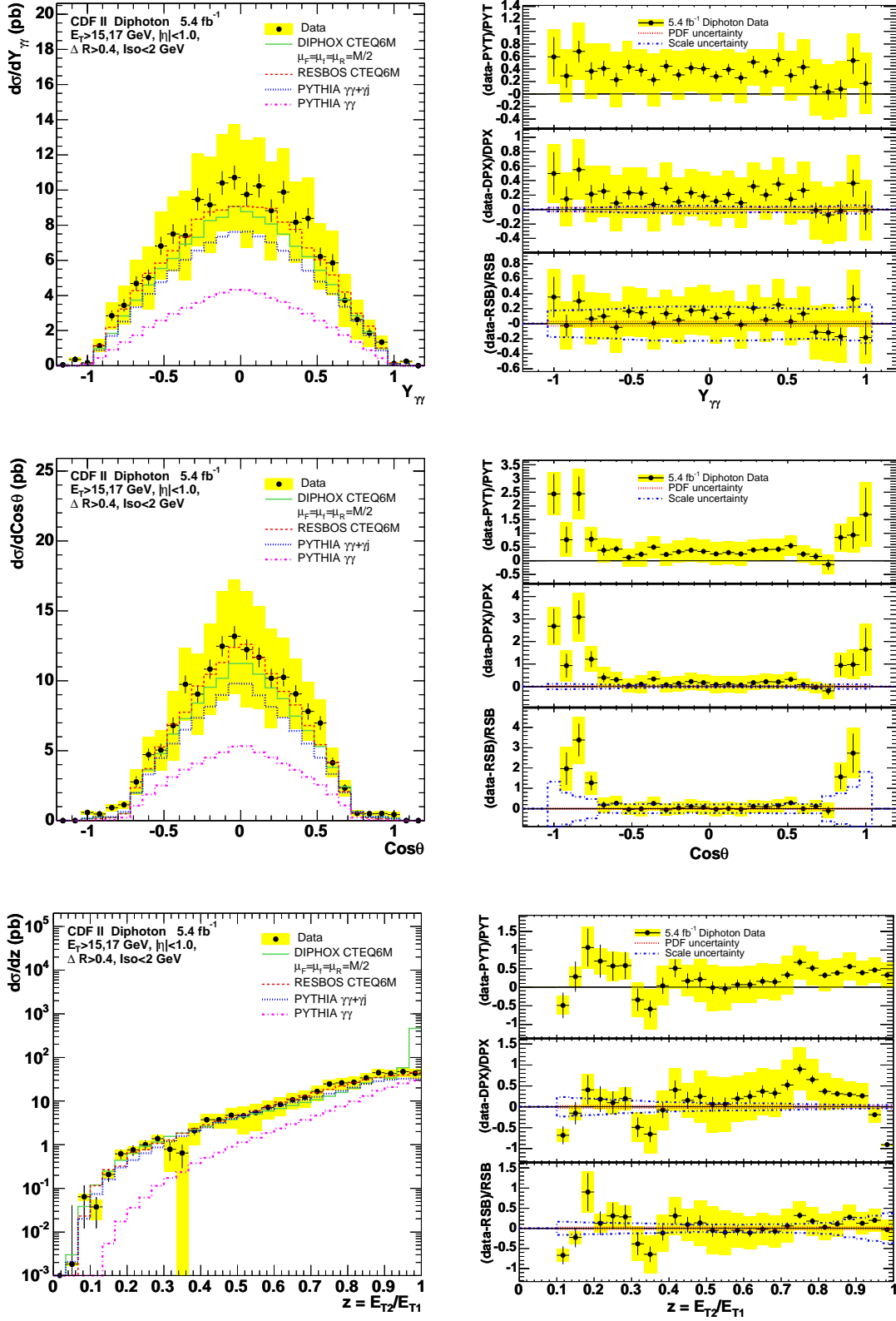
Figure 4: The measured differential cross sections compared with three theoretical predictions discussed in the text. The left windows show the absolute comparisons and the right windows show the fractional deviations of the data from the theoretical predictions. Fractional deviations for PYTHIA refer to the $\gamma\gamma + \gamma j$ calculation. Note that the vertical axis scales differ between fractional deviation plots. The comparisons are made as functions of the diphoton rapidity (top), cosine of the polar angle in the Collins-Soper frame (middle) and ratio of the subleading photon E_T to leading photon E_T (bottom). The shaded area around the data points indicates the total systematic uncertainty of the measurement.